Structure of the Analgesic μ-Conotoxin KIIIA and Effects on the Structure and Function of Disulfide Deletion[†,‡]

Keith K. Khoo,[§] Zhi-Ping Feng,[§] Brian J. Smith,[§] Min-Min Zhang,[∥] Doju Yoshikami,[∥] Baldomero M. Olivera,[∥] Grzegorz Bulaj,[⊥] and Raymond S. Norton[§,*]

The Walter and Eliza Hall Institute of Medical Research, 1G Royal Parade, Parkville, Victoria 3052, Australia, Department of Biology, University of Utah, Salt Lake City, Utah 84112, and Department of Medicinal Chemistry, College of Pharmacy, University of Utah, Salt Lake City, Utah 84108

Received October 27, 2008; Revised Manuscript Received December 17, 2008

ABSTRACT: μ-Conotoxin μ-KIIIA, from *Conus kinoshitai*, blocks mammalian neuronal voltage-gated sodium channels (VGSCs) and is a potent analgesic following systemic administration in mice. We have determined its solution structure using NMR spectroscopy. Key residues identified previously as being important for activity against VGSCs (Lys7, Trp8, Arg10, Asp11, His12, and Arg14) all reside on an α-helix with the exception of Arg14. To further probe structure−activity relationships of this toxin against VGSC subtypes, we have characterized the analogue μ-KIIIA[C1A,C9A], in which the Cys residues involved in one of the three disulfides in μ-KIIIA were replaced with Ala. Its structure is quite similar to that of μ-KIIIA, indicating that the Cys1−Cys9 disulfide bond could be removed without any significant distortion of the α-helix bearing the key residues. Consistent with this, μ-KIIIA[C1A,C9A] retained activity against VGSCs, with its rank order of potency being essentially the same as that of μ-KIIIA, namely, $Na_V1.2 > Na_V1.4 > Na_V1.7 \geq Na_V1.1 > Na_V1.3 > Na_V1.5$. Kinetics of block were obtained for $Na_V1.2$, $Na_V1.4$, and $Na_V1.7$, and in each case, both k_{on} and k_{off} values of μ-KIIIA[C1A,C9A] were larger than those of μ-KIIIA. Our results show that the key residues for VGSC binding lie mostly on an α-helix and that the first disulfide bond can be removed without significantly affecting the structure of this helix, although the modification accelerates the on and off rates of the peptide against all tested VGSC subtypes. These findings lay the groundwork for the design of minimized peptides and helical mimetics as novel analgesics.

Voltage-gated sodium channels (VGSCs)[1] play key roles in the electrical excitability of cells by regulating the influx of sodium ions. In mammals, nine different subtypes ($Na_V1.1-1.9$) have been identified, each with different distributions in the body (*1*). Of particular interest are the neuronal subtypes as several have been implicated in the perception of pain (*2*). As such, modulators of these subtypes may have potential therapeutic use as analgesics. Many peptide toxins have evolved to target VGSCs with high selectivity and potency (*1, 3*). Toxins such as ProTx-II from spiders or μO-MrVIB from marine cone snails not only provide novel analgesics but also define novel binding sites for future development of small molecules (*4*−*7*). Another group of sodium channel-blocking toxins, some of which possess analgesic activity, is made up of the μ-conotoxins, which bind to the extracellular side of the pore (site 1) and occlude the passage of sodium ions through the pore (*8, 9*).

Conotoxin μ-KIIIA from *Conus kinoshitai* belongs to a new class of μ-conotoxins that selectively block tetrodotoxin (TTX)-resistant VGSCs in amphibians, unlike previously characterized μ-conotoxins, which are selective for TTX-sensitive Na^+ channels (*10*). Recently, it was shown that μ-KIIIA blocked several subtypes of mammalian neuronal VGSCs and displayed potent analgesic activity following its systemic administration in mice (*11*). A study of structure−activity relationships in μ-KIIIA identified key residues important for its activity on the mammalian neuronal $Na_V1.2$ and skeletal muscle $Na_V1.4$ subtypes and demonstrated that the engineering of μ-KIIIA could provide subtype selective therapeutics against mammalian VGSCs for the potential treatment of pain (*11*).

[†] This work was supported in part by National Institute of General Medical Sciences Grants GM 48677 (to G.B., B.M.O., and D.Y.) and R21 NS055845 (to G.B. and D.Y.), as well as NHMRC IRIISS Grant 361646 and a Victorian State Government OIS grant. R.S.N. acknowledges fellowship support from the NHMRC.

[‡] Chemical shift assignments and the families of structures for μ-KIIIA and μ-KIIIA[C1A,C9A] have been deposited in the BioMagResBank as entries 20048 and 20049, respectively.

* To whom correspondence should be addressed: The Walter and Eliza Hall Institute of Medical Research, 1G Royal Parade, Parkville, Victoria 3052, Australia. Phone: +61 3 9345 2306. Fax: +61 3 9345 2686. E-mail: ray.norton@wehi.edu.au.

[§] The Walter and Eliza Hall Institute of Medical Research.

[∥] Department of Biology, University of Utah.

[⊥] Department of Medicinal Chemistry, College of Pharmacy, University of Utah.

[1] Abbreviations: μ-GIIIA and μ-GIIIB, μ-conotoxins GIIIA and GIIIB, respectively, from *Conus geographus*; μ-KIIIA, μ-conotoxin KIIIA from *Conus kinoshitai*; μ-KIIIA[C1A,C9A], μ-KIIIA with Cys1 and Cys9 replaced with Ala; $Na_V1.1$, $Na_V1.2$, etc., α-subunits of voltage-gated sodium channel subtype 1.1, 1.2, etc., cloned from rat (when abbreviation is preceded by an r) or mouse (when abbreviation is preceded by an m); μ-PIIIA, μ-conotoxin PIIIA from *Conus purpurascens*; μ-SIIIA, μ-conotoxin SIIIA from *Conus striatus*; μ-SmIIIA, μ-conotoxin SmIIIA from *Conus stercusmuscarum*; MD, molecular dynamics; NMR, nuclear magnetic resonance; rmsd, root-mean-square deviation; SD, standard deviation; TTX, tetrodotoxin; VGSC, voltage-gated sodium channel.

10.1021/bi801998a CCC: $40.75
Published on Web 01/26/2009

FIGURE 1: (A) Amino acid sequences of μ-conotoxins belonging to the μ-KIIIA class [μ-KIIIA (*10*), μ-SIIIA (*10, 44*), μ-SmIIIA (*37*), μ-CIIIA (*45*), μ-MIIIA (*45*), and μ-CnIIIA (*45*)]. Z represents pyroglutamate in the sequences of μ-SIIIA, μ-SmIIIA, and μ-MIIIA. (B) Amino acid sequences of μ-KIIIA and μ-KIIIA[C1A,C9A] with the disulfide connectivities indicated. All peptides are C-terminally amidated, as denoted by the asterisk.

In the development of more effective analgesics for the treatment of pain, peptides with higher subtype selectivity are of considerable interest, but it is also desirable to design minimized analogues with the aim of enhancing bioavailability and potency (*12*). μ-KIIIA is a particularly attractive ligand in these respects as it is already the smallest known μ-conotoxin, having only one residue in the first intercystine loop, as compared with five in most of the μ-conotoxins, in addition to lacking the two residues preceding the first cysteine residue in the N-terminus (Figure 1A). In the design of minimized peptides, it is important to compensate for the presence of structure-stabilizing disulfide bridges that may be removed in the process of pruning. However, in peptides with multiple disulfide bridges, not all of them are necessarily crucial for maintaining structure and activity (*13*−*16*). The role of the disulfide bonds in μ-KIIIA was investigated by eliminating individual disulfide bridges and testing each of the disulfide-deficient analogues against mammalian $Na_V1.2$ and $Na_V1.4$ (*17*). Removal of the Cys1−Cys9 disulfide bond did not significantly alter the biological activity against either VGSC subtype; removal of the Cys2−Cys15 bridge reduced activity, and deletion of the Cys4−Cys16 bridge eliminated activity. The structural consequences of removing the individual disulfide bonds, however, have not been analyzed experimentally.

In this study, we have determined the solution structure of μ-KIIIA and the structural consequences of removing the first disulfide bond (Cys1−Cys9) of μ-KIIIA by also determining the structure of its analogue, μ-KIIIA[C1A,C9A] (Figure 1B). We further characterized structure−activity relationships of μ-KIIIA by determining the activity of the disulfide-deficient analogue against a range of mammalian VGSC subtypes. Our work shows that removal of the Cys1−Cys9 disulfide only minimally affected the structure and function of this peptide, thus opening the way for further developments in the design of μ-conotoxin mimetics.

MATERIALS AND METHODS

Synthesis and Oxidative Folding. Peptides were synthesized using standard *N*-(9-fluorenyl)methoxycarbonyl (Fmoc) chemistry. The peptides were cleaved from the resin by being treated for 3−4 h with reagent K [TFA/water/ethanedithiol/phenol/thioanisole (82.5/5/2.5/5/5 by volume)]. The cleaved peptides were filtered, precipitated with cold methyl *tert*-butyl ether (MTBE), and washed several times with cold MTBE. The reduced peptides were purified by reversed-phase HPLC using a semipreparative C18 Vydac column (218TP510, 10 mm × 250 mm) eluted with a linear gradient from 5 to 35% solvent B in 35 min, where solvent A was 0.1% (v/v) TFA in water and solvent B was 0.1% (v/v) TFA in 90% aqueous acetonitrile (ACN). The flow rate was 5 mL/min, and absorbance was monitored at 220 nm.

To prepare μ-KIIIA analogues with the native disulfide connectivity, the first cysteine pair was protected by *S*-trityl groups and the second pair was protected by acetamidomethyl groups. To oxidize the first disulfide bridge, the reduced peptides (at a final concentration of 20 μM) were dissolved in 0.01% TFA and added to the folding mixture containing 0.1 M Tris-HCl, 1 mM EDTA, 1 mM oxidized glutathione (GSSG), and 1 mM reduced glutathione (GSH). The reactions were carried out at room temperature. After 1 h, the reactions were quenched with formic acid (final concentration of 8%) and purified by semipreparative HPLC as described above. To remove the acetamidomethyl groups from the second pair of cysteines and close the remaining disulfide bridge, the peptides were treated with 2 mM iodine in 50% aqueous acetonitrile for 10 min and the reactions quenched with ascorbic acid. The analytical HPLC gradient was linear from 5 to 35% solvent B over 35 min, where solvent A was 0.1% (v/v) TFA in water and solvent B was 0.1% (v/v) TFA in 90% aqueous acetonitrile. The flow rate was 1 mL/min. The identities of final products were confirmed by MALDI-TOF analysis.

NMR Spectroscopy. NMR spectra were recorded with a 2.6 mM solution of μ-KIIIA (pH 2.9 and 4.8) and a 3.7 mM solution of μ-KIIIA[C1A,C9A] (pH 3.2 and 5.3) in 94% H_2O/6% ^2H_2O and 95% H_2O/5% ^2H_2O mixtures, respectively. For each of the peptides, a series of one-dimensional (1D) spectra at 5 °C intervals was collected over the temperature range of 5−25 °C. Two-dimensional homonuclear total correlation (TOCSY) spectra with a spin-lock time of 70 ms, nuclear Overhauser enhancement (NOESY) spectra with mixing times of 50 and 250 ms, and double-quantum-filtered correlation (DQF-COSY) spectra were acquired at 600 MHz on a Bruker DRX-600 spectrometer. NOESY spectra (250 ms) were also recorded at 20 °C for both peptides to confirm assignments in the event of peak overlap. In addition, $^1H-^{13}C$ HSQC spectra for the assignment of ^{13}C chemical shifts were collected at 5 °C on the Bruker DRX-600 instrument, and $^1H-^{15}N$ HSQC spectra for the assignment of ^{15}N chemical shifts (*18, 19*) were collected on a Bruker Avance 500 spectrometer equipped with a TXI cryoprobe. Diffusion measurements were performed at 5 and 20 °C using a pulsed field gradient longitudinal eddy-current delay pulse sequence (*20, 21*) as implemented by Yao et al. (*22*). The water resonance was suppressed using the WATERGATE pulse sequence (*23*). Amide exchange rates were monitored by dissolving freeze-dried material in ^2H_2O at pH 5.2 for μ-KIIIA and pH 4.2 for μ-KIIIA[C1A,C9A] and then recording a series of one-dimensional 1D spectra, followed by 70 ms TOCSY and 50 ms NOESY. All spectra were acquired at 5 °C unless otherwise stated and were referenced via the water resonance. Spectra were processed using

Table 1: Structural Statistics for μ-KIIIA and μ-KIIIA[C1A,C9A]

	μ-KIIIA	μ-KIIIA[C1A,C9A]
no. of distance restraints	225	241
intra ($i = j$)	97	100
sequential ($\|i - j\| = 1$)	70	55
short-range ($1 < \|i - j\| < 6$)	45	69
long-range	13	17
no. of dihedral restraints	8	6
energies (kcal/mol)[a]		
E_{NOE}	1.6 ± 0.3	2.2 ± 0.4
deviations from ideal geometry[b]		
bonds (Å)	0.0017 ± 0.0002	0.0018 ± 0.0002
angles (deg)	0.503 ± 0.013	0.531 ± 0.017
impropers (deg)	0.371 ± 0.009	0.403 ± 0.016
mean global rmsd (Å)[c]		
backbone heavy atoms		
all residues	0.58 ± 0.11	0.97 ± 0.38
residues 5−16 [$S(\psi)$, $S(\phi) > 0.8$]	0.45 ± 0.12	0.54 ± 0.11
all heavy atoms		
all residues	1.42 ± 0.28	1.77 ± 0.42
residues 5−16 [$S(\psi)$, $S(\phi) > 0.8$]	1.44 ± 0.31	1.55 ± 0.42
Ramachandran plot[d]		
most favored (%)	78.9	76.1
allowed (%)	21.1	22.9
additionally allowed (%)	0	1.1
disallowed (%)	0	0

[a] The values for E_{NOE} were calculated from a square well potential with force constants of 50 kcal mol^{-1} Å^2. [b] The values for the bonds, angles, and impropers show the deviations from ideal values based on perfect stereochemistry. [c] The pairwise rmsd over the indicated residues calculated in MOLMOL. [d] As determined with PROCHECK-NMR for all residues except Gly and Pro.

TOPSPIN (version 1.3, Bruker Biospin) and analyzed using XEASY (version 1.3.13) (*24*).

Structural Constraints. $^3J_{HNH\alpha}$ coupling constants were measured from DQF-COSY spectra at 600 MHz and then converted to dihedral restraints as follows: $^3J_{HNH\alpha} > 8$ Hz, $\phi = -120 \pm 40°$; $^3J_{HNH\alpha} < 6$ Hz, $\phi = -60 \pm 40°$. Five ϕ angles (Lys7−Asp11) were restrained in both peptides. χ^1 angles for some residues were determined on the basis of analysis of a short mixing time (50 ms) NOESY spectrum. Three χ^1 angles (Cys4, Arg10, and His12) were constrained in final structure calculations of μ-KIIIA, and one (Cys15) was constrained in μ-KIIIA[C1A,C9A]. The final constraints are summarized in Table 1, and details have been deposited in the BioMagResBank (*25*) as entries 20048 and 20049 for μ-KIIIA and μ-KIIIA[C1A,C9A], respectively.

Structure Calculations. Intensities of NOE cross-peaks were measured in XEASY and calibrated using the CALIBA macro of CYANA (version 1.0.6) (*26*). NOEs providing no restraint or representing fixed distances were removed. The constraint list resulting from the CALIBA macro of CYANA was used in Xplor-NIH to calculate a family of 200 structures using the simulated annealing script (*27*). The 60 lowest-energy structures were then subjected to energy minimization in water; during this process, a box of water with a periodic boundary of 18.856 Å was built around the peptide structure and the ensemble was energy-minimized on the basis of NOE and dihedral restraints and the geometry of the bonds, angles, and impropers. From this set of structures, final families of 20 lowest-energy structures were chosen for analysis using PROCHECK-NMR (*28*) and MOLMOL (*29*). In all cases, the final structures had no experimental distance violations greater than 0.2 Å or dihedral angle violations greater than 5°. Structural figures were prepared using MOLMOL (*29*) and PyMOL (*47*).

Comparative Modeling and Molecular Dynamics. Models of μ-KIIIA and three disulfide-deficient analogues (μ-KIIIA-[C1A,C9A], μ-KIIIA[C2A,C15A], and μ-KIIIA[C4A,C16A]) were generated from the solution structure of the closely related μ-conotoxin μ-SmIIIA (Protein Data Bank entry 1Q2J) using the MODELLER (8v2) software (*30*) by homology modeling methods. The 20 experimental NMR structures of μ-SmIIIA (*31*) were used to generate the initial models based on the sequence alignment in Figure 1. For each initial alignment, 25 models were generated, and from each of these 25 models, the model with the lowest MODELLER Objective Function was used in the molecular dynamics (MD) calculations. Models of the three disulfide-deficient analogues were also generated using the solution structure of μ-KIIIA (determined in this study) as an initial template. Initial models of each analogue were constructed from the ensemble of experimental NMR structures of μ-KIIIA, and the structure with the lowest MODELLER Objective Function was used in subsequent MD calculations. As the results for the three disulfide-deficient analogues were largely independent of which starting structure was used (μ-SmIIIA vs μ-KIIIA), only one set of structures (those starting from μ-KIIIA) is described in detail in Results.

MD simulations were conducted using the GROMACS version 3.3.1 package of programs (*32*) employing the OPLS-aa force field (*33*). The toxins were solvated in a box of water, and the total charge of the system was made neutral by replacing water molecules with chloride ions. The LINCS algorithm was used to constrain bond lengths (*34*). Peptide, water, and ions were coupled separately to a thermal bath at 300 K using a Berendsen thermostat (*35*) applied with a coupling time of 0.1 ps. All simulations were performed with a single nonbonded cutoff of 10 Å, applying a neighbor-list update frequency of 10 steps (20 fs). The particle mesh Ewald method was applied to deal with long-range electrostatics with a grid width of 1.2 Å and fourth-order spline interpolation. All simulations consisted of an initial minimization to remove close contacts, followed by positional restrained MD for 10 ps to equilibrate the water molecules with the polypeptide fixed. The time step used in all the simulations was 2 fs. MD simulations for each peptide were run for a total time of 50 ns. Structures were extracted from the trajectory of each MD simulation at time intervals of 0.2 ns. A comparison of the rmsd of the superposition of backbone atoms between all extracted structures is presented as heat maps (Figure S7 of the Supporting Information), illustrating the structural variation observed during the simulations. Cluster analysis was performed using the method of Daura et al. (*36*) to select representative conformers sampled throughout the simulation.

Electrophysiology of Mammalian Na_V Clones Expressed in Xenopus *Oocytes*. Oocytes expressing VGSCs were prepared and two-electrode voltage clamped essentially as described previously (*11*). Briefly, oocytes were placed in a 30 μL chamber containing ND96 and two-electrode voltage clamped at a holding potential of −80 mV. To activate VGSCs, the membrane potential was stepped to a value between −20 and 0 mV (depending on Na_V subtype) for a 50 ms period every 20 s. To apply toxin, the perfusion was halted, 3 μL of toxin solution (at 10 times the final concentration) was applied to the 30 μL bath, and the bath was manually stirred for ~5 s by gently aspirating and expelling a few microliters of the bath fluid several times with a pipettor. Toxin exposures were in static baths to

conserve material. On-rate constants were obtained assuming the equation $k_{obs} = k_{on}$[peptide] + k_{off} (*37*), where k_{obs} was determined from the single-exponential fit of the time course of block by a fixed concentration of 1 μM peptide and k_{off} determined from single-exponential fits of the time course of recovery from block following toxin washout. All recordings were made at room temperature (~21 °C).

RESULTS

NMR Spectroscopy. Good-quality spectra were obtained for both μ-KIIIA and μ-KIIIA[C1A,C9A]. Broad NH chemical shift dispersion for both peptides indicated that both were well structured and adopted a single major conformation in solution. The amide and aromatic regions of 1D spectra of μ-KIIIA and μ-KIIIA[C1A,C9A] at different temperatures are shown in Figure S1 of the Supporting Information and the fingerprint regions of TOCSY and NOESY spectra in Figure S2. Chemical shift assignments are presented in Tables S1 and S2 of the Supporting Information and have been deposited in the BioMagResBank (*25*) as entries 20048 and 20049 for μ-KIIIA and μ-KIIIA[C1A,C9A], respectively. Distance restraints were obtained from the intensities of the NOE cross-peaks at 5 °C and pH 4.8 for μ-KIIIA and 5 °C and pH 5.3 for μ-KIIIA[C1A,C9A], with NOESY spectra at higher temperatures and lower pH being used to resolve peak overlap.

Self-diffusion coefficients of μ-KIIIA and μ-KIIIA[C1A, C9A] at 5 °C are (1.71 ± 0.03) × 10^{-10} m^2 /s (SD over 12 resonances) and (1.80 ± 0.09) × 10^{-10} m^2/s (SD over eight resonances), respectively. These values were similar to that of α-RgIA (*38*), a 13-residue α-conotoxin with a well-defined structure. Extrapolated values were comparable (~18% faster) to those obtained for peptides studied by Yao et al. (*22*), indicating that both μ-KIIIA and μ-KIIIA[C1A,C9A] were monomeric and structurally compact in solution.

Deviations of the backbone NH and H^{α} chemical shifts of μ-KIIIA and μ-KIIIA[C1A,C9A] from random coil values (*39*) are plotted in Figure 2. The similarities in the pattern of deviations confirm that they adopt similar backbone structures. Differences in backbone NH and H^{α} chemical shifts between μ-KIIIA and μ-KIIIA[C1A,C9A] are also plotted, the largest deviations occurring at the N- and C-termini, as well as the region around residue 9. The perturbations of Ser13, Arg14, Cys15, and Cys16 imply that the C-terminal region is slightly affected by removal of the Cys1−-Cys9 disulfide, presumably because of the proximity of the N- and C-termini engendered by the Cys2−Cys15 disulfide (see below).

Solution Structures. A summary of experimental constraints and structural statistics for μ-KIIIA and μ-KIIIA-[C1A,C9A] is given in Table 1. The angular order parameters for ϕ and ψ in the final ensemble of 20 structures for μ-KIIIA were both >0.8 over all residues (Figure S3 of the Supporting Information), indicating that these backbone dihedral angles are well-defined across the family of structures. For μ-KIIIA[C1A,C9A], the corresponding angular order parameters were >0.8 over residues 5−16. The mean pairwise rms differences over the backbone heavy atoms over all residues for the families of structures of μ-KIIIA and μ-KIIIA[C1A,C9A] were 0.58 and 0.97 Å, respectively. Over residues 5−16, the rms differences were 0.45 and 0.54 Å,

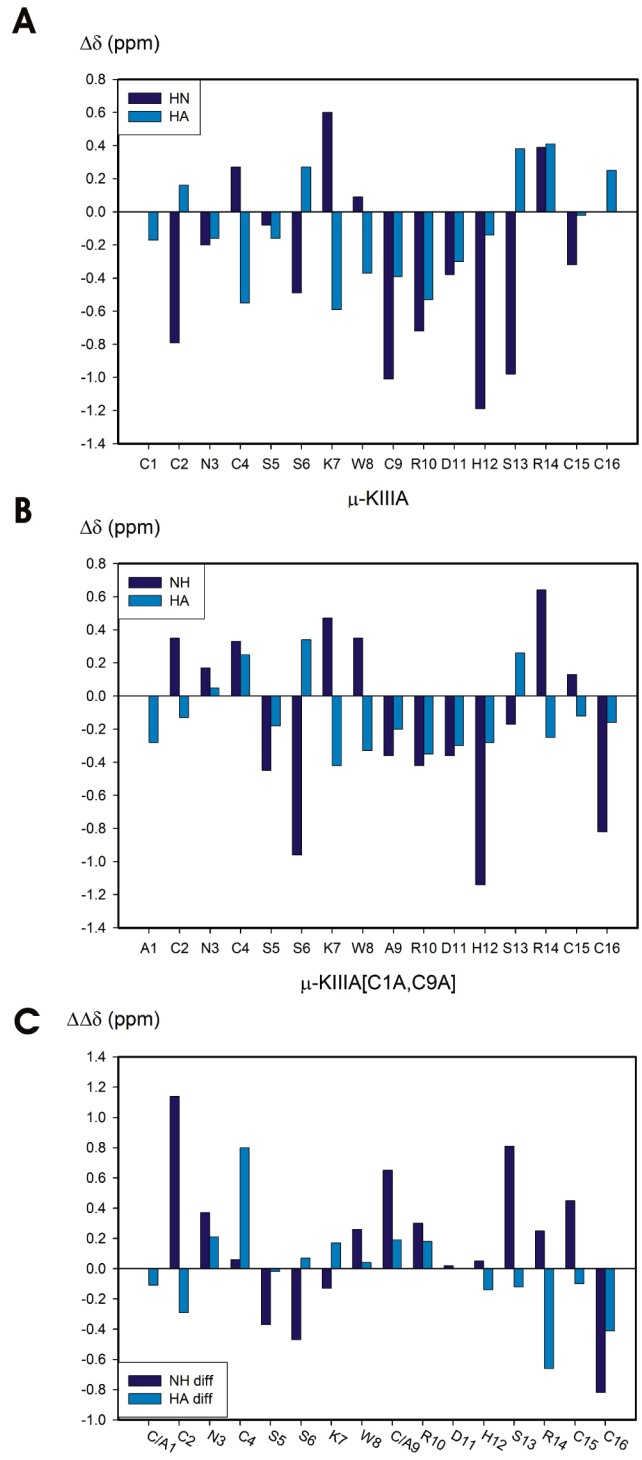

FIGURE 2: Chemical shift deviation of backbone amide and C^{α} protons from random coil values at 5 °C (*39*) for (A) μ-KIIIA and (B) μ-KIIIA[C1A,C9A]. Random coil values for oxidized Cys residues were obtained from ref *46*. (C) Chemical shift differences in backbone amide and C^{α} protons between μ-KIIIA and μ-KIIIA[C1A,C9A] at 5 °C.

respectively (Figure 3). The closest-to-average structures of both μ-KIIIA and μ-KIIIA[C1A,C9A] are characterized by an α-helix from Lys7 to His12, which was present in 16 of 20 structures of μ-KIIIA and 18 of 20 structures of μ-KIIIA[C1A,C9A]. The presence of medium-range NOEs [$d_{\alpha N}(i, i + 3)$ and $d_{\alpha N}(i, i + 4)$] in this region supports the helix observed (Figure S4 of the Supporting Information). The locations of side chains in the families of structures are

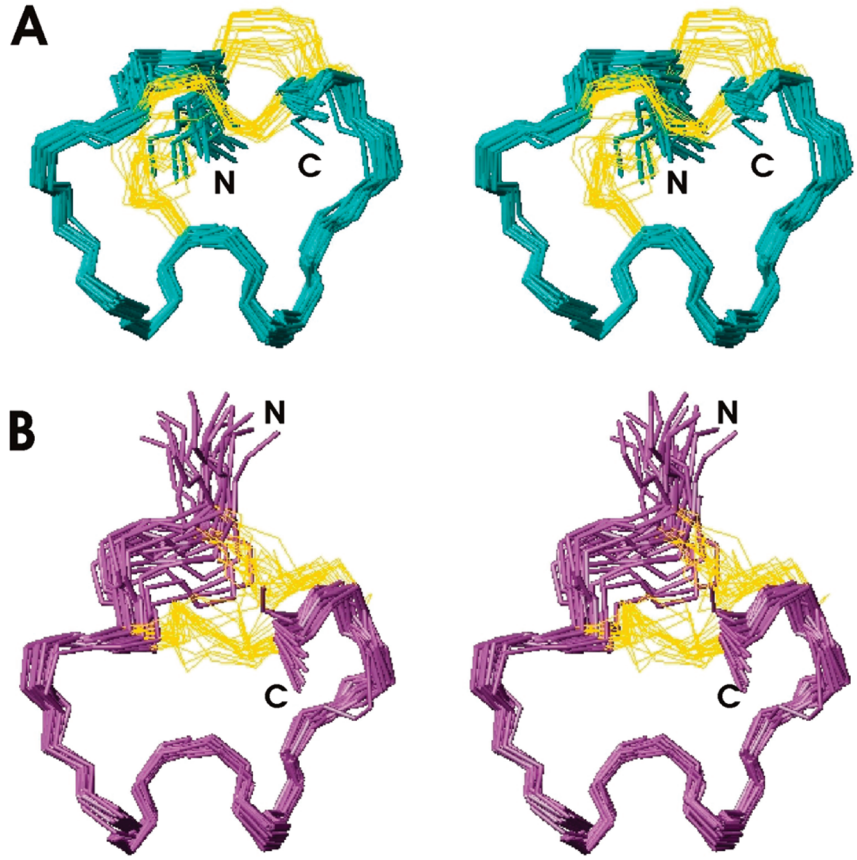

FIGURE 3: Stereoviews of a family of 20 final structures for (A) μ-KIIIA and (B) μ-KIIIA[C1A,C9A] superimposed over backbone heavy atoms (N, C^{α}, and C′) over residues 5−16 with disulfide bonds colored gold.

shown in Figure S5 of the Supporting Information. Hydrogen bonds were observed from Arg10 NH to Ser6 O and from Asp11 NH to Lys7 O in all 20 structures of μ-KIIIA[C1A, C9A]. Hydrogen bonds from Arg10 NH to Ser6 O were observed in all 20 structures of μ-KIIIA, while Asp11 NH to Lys7 O hydrogen bonds were observed in 18 of 20 structures.

Comparison of μ-KIIIA and μ-KIIIA[C1A,C9A]. Figure 4 shows a superposition of the closest-to-average structures of μ-KIIIA and μ-KIIIA[C1A,C9A] over the backbone heavy atoms of residues 5−16. The backbones generally align well over these residues, with a pairwise rmsd of 0.95 Å, and adopt a very similar secondary structure, with an α-helix from residue 7 to 12. The key residues for VGSC binding identified by Zhang et al. (*11*) (Lys7, Trp8, Arg10, Asp11, His12, and Arg14) mostly lie in the α-helical region and occupy similar positions in μ-KIIIA and μ-KIIIA[C1A,C9A], although the orientation of the Trp8 and His12 side chains differs slightly between the two peptides. This difference between the relative orientations of these two key side chains may reflect differences in the NOE restraint sets for the two peptides as a result of peak overlap, since the side chain chemical shifts, which are a sensitive indicator of local environment, especially for aromatic side chains, are very similar for μ-KIIIA and μ-KIIIA[C1A,C9A] (Tables S1 and S2 of the Supporting Information).

Structurally, the main difference lies in the conformation of the N-terminal region, which, in μ-KIIIA[C1A,C9A], is no longer constrained by a disulfide bond to the α-helical region and, as a result, appears to be more flexible. A comparison of the number of NOEs (Figures S2 and S3 of the Supporting Information) in the N-terminal region showed that μ-KIIIA[C1A,C9A] had fewer NOE restraints for residues 1−3 than μ-KIIIA, although a greater total number of distance restraints was obtained for μ-KIIIA[C1A,C9A] because of its higher concentration compared with that of μ-KIIIA. Peak overlap of amide resonances from residues 2−4 in the μ-KIIIA[C1A,C9A] NOESY spectrum complicated an accurate comparison of N-terminal (residues 1−4) NOEs in the two spectra, but strong sequential NOEs from the amide of Cys2 to C^{β} protons of Cys1 and a long-range NOE from the amide of Asn3 to the C^{β} proton of Cys9 seen in the μ-KIIIA spectra were clearly absent in the spectrum of μ-KIIIA[C1A,C9A] (Figure S2 of the Supporting Information). To confirm that the disorder observed in the N-terminal of μ-KIIIA[C1A,C9A] was not simply the result of a lack of NOEs, other parameters were also compared. As mentioned above, the backbone ^{1}H chemical shifts indicated significant differences in the N-terminal region (Figure 2). A comparison of ^{13}C chemical shifts (Figure S6 of the Supporting Information) gave similar results, consistent with a change in conformation of both the N-terminal and C-terminal regions as a result of removal of the disulfide bond. Finally, $^{3}J_{\mathrm{HNH}\alpha}$ for Cys4 in μ-KIIIA[C1A,C9A] was >8 Hz, as compared to 6.1 Hz for the same residue in μ-KIIIA, suggesting a more extended conformation for this residue in μ-KIIIA[C1A,C9A] than in μ-KIIIA.

Molecular Dynamics. Molecular dynamics simulations on μ-KIIIA and each of the disulfide-deficient analogues were conducted to examine the likely structural consequences of removing individual disulfide bonds. Figure 5 shows a comparison of the representative structures sampled through-

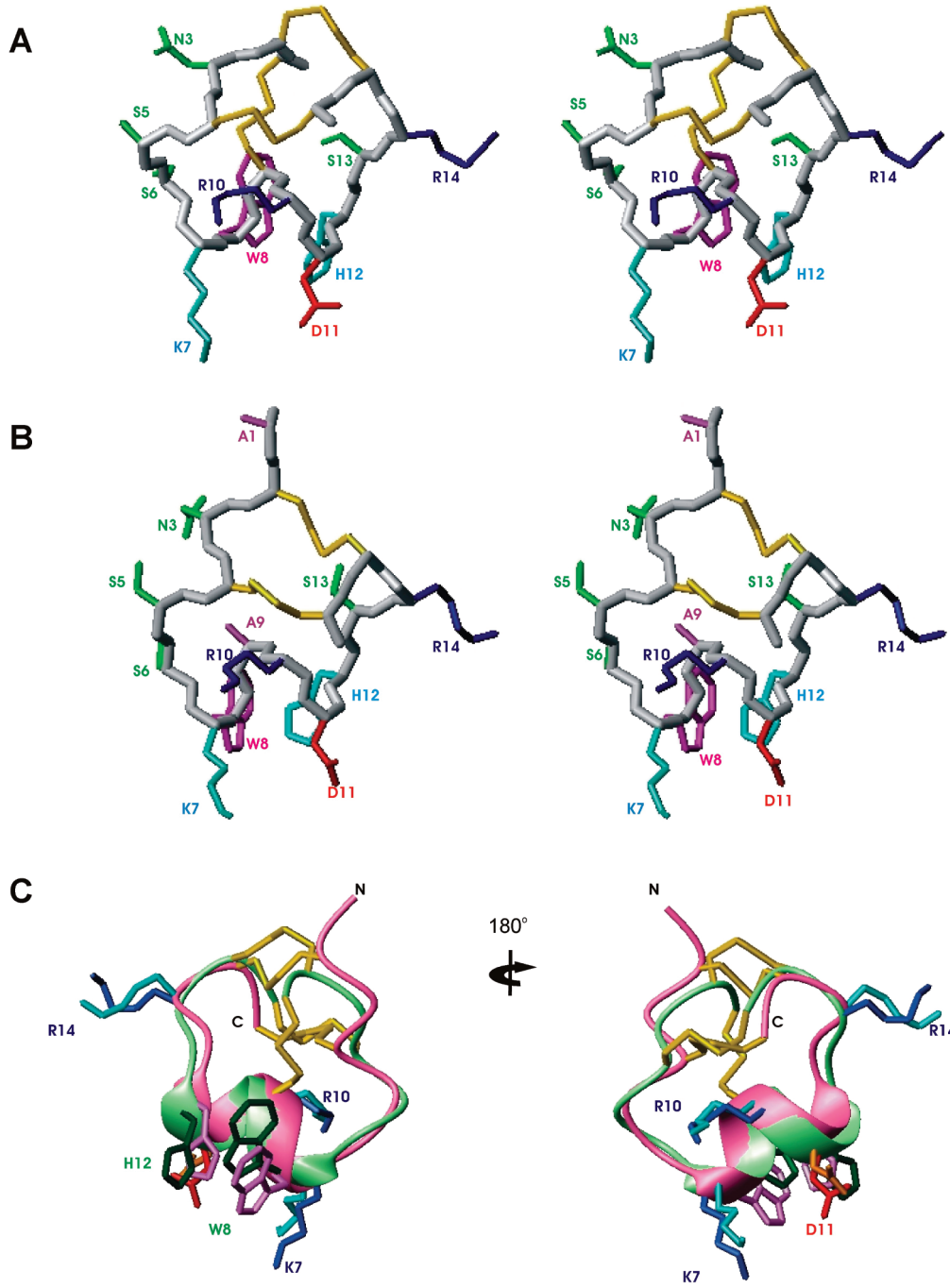

FIGURE 4: Stereoviews of the closest-to-average structures of (A) μ-KIIIA and (B) μ-KIIIA[C1A,C9A] with all side chain heavy atoms displayed and labeled. Disulfide bonds are colored gold; positively charged residues are colored blue, negatively charged residues red, hydrophilic residues green, and aromatic residues magenta. (C) Structural overlay of the closest-to-average structures of μ-KIIIA (green) and μ-KIIIA[C1A,C9A] (purple) over the backbone heavy atoms of residues 5−16. Disulfide bonds are colored gold, and side chains of key residues are shown; positively charged residues are colored blue and negatively charged residues red. The two views are related by a 180° rotation about the vertical axis.

out the 50 ns of MD simulations of μ-KIIIA and μ-KIIIA-[C1A,C9A] with the ensemble of NMR-determined structures. The comparison shows that for both peptides the ensemble of MD-simulated structures adopted an overall fold similar to that of the experimentally derived structures. Similar results (not shown) were obtained using models that employed μ-SmIIIA as a template in the comparative modeling of the structures used to initiate the MD calculations. The conformity of these results highlights the utility of comparative modeling and molecular dynamics in structural studies of small toxins.

The structural variability of each peptide during the MD simulation is presented as rmsd plots (Figure S7 of the Supporting Information). The rmsd plot for μ-KIIIA indicates this peptide is significantly less flexible and therefore explores less conformational space than the other peptides. The most representative structure from the MD simulations of each peptide is shown in Figure S8 of the Supporting Information. For μ-KIIIA, μ-KIIIA[C1A,C9A], and μ-KIIIA-[C2A,C15A], an α-helix was observed from Lys7 to Asp11 or His12. The structure of μ-KIIIA[C4A,C16A] showed the largest variation of all the peptides; during the latter half of

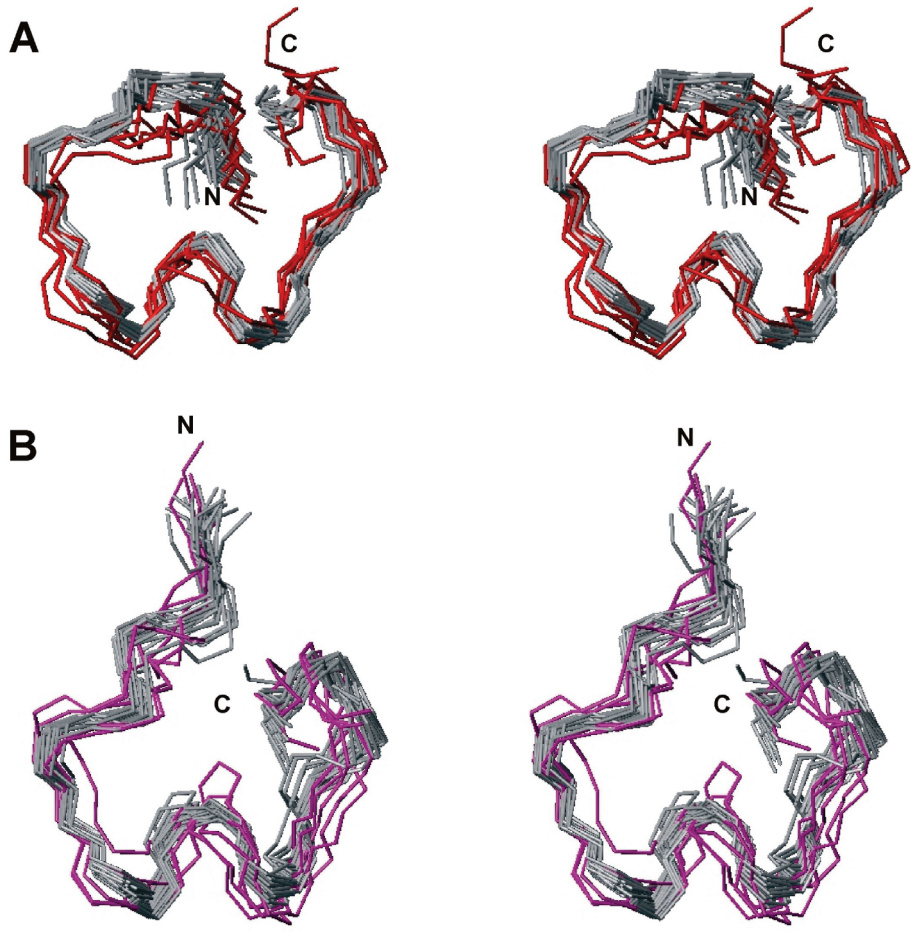

FIGURE 5: Stereoviews of (A) representative MD structures (red) and NMR structures (gray) of μ-KIIIA and (B) representative MD structures (magenta) and NMR structures (gray) of μ-KIIIA[C1A,C9A]. Structures are superimposed over backbone heavy atoms (N, C^{α}, and C′) over residues 4−16. The MD structures of μ-KIIIA were generated using μ-SmIIIA as a starting structure, whereas those for μ-KIIIA[C1A,C9A] were generated from the μ-KIIIA structure determined experimentally in this study.

Table 2: Block by 1 μM μ-KIIIA[C1A,C9A] of Cloned VGSCs[a]

channel[b]	% block[c]	k_{obs} (min^{-1})	k_{off} (min^{-1})	k_{on}[d] (μM^{-1} min^{-1})	K_d[e] (μM)	μ-KIIIA K_d[f] (μM)
$rNa_V1.1$	3 ± 2	NA[g]	NA	−	−	0.29 ± 0.11
$rNa_V1.2$	93 ± 2	1.8 ± 0.39	0.014 ± 0.002	1.8 ± 0.39	0.008 ± 0.002	0.005 ± 0.005
$rNa_V1.3$	7 ± 2	NA	NA	−	−	4.6 ± 1.5
$rNa_V1.4$	85 ± 2	4.0 ± 0.5	0.78 ± 0.1	3.22 ± 0.51	0.24 ± 0.05	0.05 ± 0.016
$rNa_V1.5$	1 ± 2	NA	NA	−	−	−
$rNa_V1.6$	82 ± 2	0.48 ± 0.07	0.08 ± 0.015	0.4 ± 0.071	0.2 ± 0.05	−[h]
$mNa_V1.7$	27 ± 1	0.72 ± 0.4	0.37 ± 0.09	0.35 ± 0.41	1.1 ± 1.3	0.29 ± 0.09

[a] Values (mean ± SD, $n \geq 3$) were obtained by two-electrode voltage clamp of *Xenopus* oocytes expressing cloned channels as described in Materials and Methods. Results for $rNa_V1.2$ and $rNa_V1.4$ are from ref *17*. [b] α-Subunit cloned from rat (r) or mouse (m). [c] Steady-state block of peak sodium current. [d] From $k_{obs} - k_{off}$. [e] From k_{off}/k_{on}. [f] Values for wild-type μ-KIIIA are from ref *11*. [g] Unable to be determined because block was too small and apparent kinetics too fast for accurate measurement. [h] Block of $Na_V1.6$ by wild-type μ-KIIIA was only partially reversible and precluded K_d determination (*11*).

the MD simulation, the helix was replaced by random coil, yielding a structure with a very different, albeit relatively stable, conformation compared with the other three peptides.

Functional Activity in Blocking VGSCs. The ability of μ-KIIIA[C1A,C9A] to block cloned α-subunits of rat (r) or mouse (m) sodium channels expressed in oocytes was assessed by voltage-clamp protocols. The peptide was shown recently to readily block $Na_V1.2$, a neuronal subtype, and $Na_V1.4$, a skeletal muscle subtype (*17*); here we have investigated five additional channel subtypes. Table 2 summarizes the activity of μ-KIIIA[C1A,C9A] against all seven VGSC subtypes tested, including neuronal subtypes $Na_V1.1$, -1.2, -1.3, -1.6, and -1.7 and heart muscle subtype $rNa_V1.5$. In addition to $rNa_V1.2$ and -1.4, $mNa_V1.6$ and $rNa_V1.7$ were readily blocked by μ-KIIIA[C1A,C9A], with estimated K_d values ranging from 8 nM to 1.1 μM, while the remaining Na_V subtypes were minimally blocked. To conserve material, the K_d values shown in Table 2 were estimated from the kinetics of block and recovery employing a single concentration (1 μM) of peptide; this appears to be justified insofar as the K_d values were all within a factor of 3 of the IC_{50} values predicted from steady-state block (cf. the second column of Table 2), assuming the Langmuir absorption isotherm, % block = 100 × plateau/(1 + IC_{50}/[toxin]). The value used for plateau was 1.0 in all cases except $Na_V1.2$, where 0.95 was used instead since a 5%

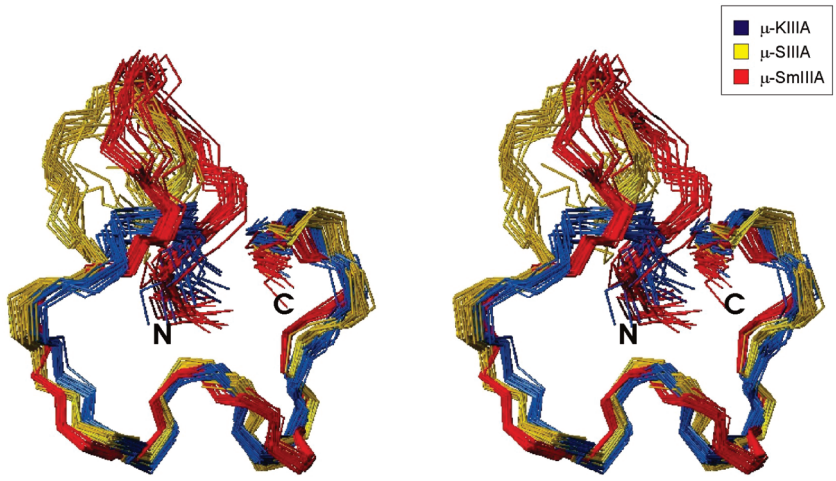

FIGURE 6: Stereoviews of families of 20 final structures of μ-KIIIA (blue), μ-SIIIA (yellow) (BMRB accession number 20023) and μ-SmIIIA (red) (PDB entry 1Q2J) superimposed over backbone heavy atoms (N, C^{α}, and C′) of residues 4−16 for μ-KIIIA (residues 8−20 for μ-SIIIA and residues 10−22 for μ-SmIIIA).

residual current is observed with saturating concentrations of μ-KIIIA on $Na_V1.2$ (*40*) and assuming μ-KIIIA[C1A, C9A] has a similar residual current. The predicted IC_{50} values were 0.022, 0.18, 0.22, and 2.7 μM for $Na_V1.2$, -1.4, -1.6, and -1.7, respectively.

On the basis of % block and/or K_d values, the disulfide-deleted peptide blocked $Na_V1.2$ best, with the following rank order of potency: $rNa_V1.2 > rNa_V1.4 \approx mNa_V1.6 > rNa_V1.7 > rNa_V1.1 \approx rNa_V1.3 > rNa_V1.5$. For comparison, the previously determined K_d values of wild-type μ-KIIIA are also listed in Table 2; its rank order of potency is as follows: $rNa_V1.2 > rNa_V1.4 > rNa_V1.1 \approx rNa_V1.7 > rNa_V1.3 > rNa_V1.5$ ($mNa_V1.6$ is absent because its block was only partially reversible) (*11*). μ-KIIIA blocked $rNa_V1.2$, -1.4, and -1.7 with k_{on} values of 0.3, 0.97, and 0.024 μM^{-1} min^{-1}, respectively, and k_{off} values of 0.0016, 0.047, and 0.007 min^{-1}, respectively (*11*). Comparison of these values with those of μ-KIIIA[C1A,C9A] in Table 2 reveals that, in each case, the disulfide deletion increased both k_{on} and k_{off} of the peptide.

DISCUSSION

In this study, we have determined the solution structures of μ-KIIIA and its disulfide-deficient analogue μ-KIIIA-[C1A,C9A] to investigate the structural and functional consequences of removing the first disulfide bond (Cys1−Cys9). We begin by comparing the structure of μ-KIIIA with those of the closely related μ-conotoxins, μ-SIIIA and μ-SmIIIA, and then consider the implications of our findings with respect to the effect of disulfide deletion for generation of minimized analogues and mimetics of μ-KIIIA.

Comparison of μ-KIIIA with μ-SIIIA and μ-SmIIIA. μ-KIIIA was characterized previously as belonging to the same class of μ-conotoxins as μ-SIIIA and μ-SmIIIA, with the three peptides having an essentially identical C-terminal region but differing in the length of the first N-terminal loop (*10*) (Figure 1). In that study, molecular dynamics simulations were used to model the structures of μ-KIIIA and μ-SIIIA from μ-SmIIIA and to analyze the structural consequence of altering the number of residues in the first loop (*10*). The solution structure of μ-SmIIIA was described a few years ago by Keizer et al. (*31*), while the solution structure of μ-SIIIA has been determined recently by two different groups (*41, 42*). Comparing the solution structures of these three μ-conotoxins confirmed the results of the MD simulations in that the number of residues in the first loop did not affect the overall conformations of the second and third loops (*10*). Superimpositions of the three structures over the backbone heavy atoms of the second and third loops (residues 4−16 of μ-KIIIA) gave a mean global pairwise rmsd of 0.92 Å, with μ-KIIIA being more similar to μ-SIIIA (group rmsd of 0.88 Å) than μ-SmIIIA (group rmsd of 1.34 Å), as illustrated in Figure 6. As in μ-KIIIA, the secondary structures of μ-SIIIA (*41, 42*) and μ-SmIIIA (*31*) were characterized by an α-helix corresponding to residues 7−12 of μ-KIIIA, although in μ-SmIIIA this helix was somewhat distorted. As expected, the main difference lies in the length of the first inter-cysteine loop toward the N-terminus, which, in all three peptides, is oriented away from the C-terminal region. This is in marked contrast to the solution structure of μ-SIIIA described recently by Schroeder et al. (*41*), which shows this loop projecting inward, under the Cys4−Cys16 disulfide bridge and toward the α-helix. As the structural statistics for this structure were not published and the structure is not available from BMRB, a detailed comparison with the other structures is not possible.

Key Residues Lie on an α-Helix. Our structure of μ-KIIIA shows that the key residues important for activity against $Na_V1.2$ and $Na_V1.4$, as identified recently by Zhang et al. (*11*), all reside on the α-helical region of the peptide, with the exception of Arg14. This was also the case for μ-SIIIA, suggesting an important role for the α-helix in presenting these residues to mammalian sodium channels (*41*). Our results for μ-KIIIA[C1A,C9A] also demonstrate that the Cys1−Cys9 disulfide bond can be removed without significantly distorting the α-helix and with minimal change in the activity of the peptide against the $Na_V1.2$ subtype and only slight reductions in affinity for the $Na_V1.4$ and $Na_V1.7$ subtypes, in spite of the apparent flexibility of the N-terminus imparted by removal of the disulfide bond. As the disulfide-deficient analogue maintains activity similar to that of the native toxin, this suggests that the conformation of the N-terminal region is not critical in maintaining the structure and activity of the peptide against the $Na_V1.2$ subtype.

However, this flexibility may influence the selectivity profile of the toxin for other Na_V subtypes, such as $Na_V1.4$ and $Na_V1.7$. Interestingly, μ-SIIIA, which has a longer N-terminal loop, reportedly does not target the $Na_V1.1$ and $Na_V1.7$ subtypes (*41*).

Although there was minimal change in the activity against $Na_V1.2$ and $Na_V1.4$ upon removal of the Cys1−Cys9 disulfide bridge, the disulfide deletion increased both k_{on} and k_{off} of the peptide against these subtypes. Interestingly, disulfide deletion also increased the kinetics of peptide binding to its target channel in the case of conkunitzin-S1 (*43*), a neurotoxin that binds voltage-gated potassium channels. In that study, addition of a disulfide bond to the native toxin decreased both k_{on} and k_{off} for binding of the toxin to the *Shaker* potassium channel target but did not affect the overall blocking activity against this channel. These results suggest that the enhanced flexibility of a peptide toxin conferred by removing a conformational restraint such as a disulfide bridge may enhance its ability to both associate with and dissociate from its target channel. It is also possible that the slightly more expanded and flexible N-terminal region of μ-KIIIA[C1A,C9A] compared with μ-KIIIA may enable it to sample a larger volume of conformational space and thereby facilitate eventual binding to the channel.

The relationship between conformational flexibility and binding is supported by the MD simulations; removal of the Cys1−Cys9 and Cys2−Cys15 disulfide bridges resulted in analogues that were more conformationally flexible than the native toxin but still retained activity against the VGSCs, albeit with lower affinity (*17*). In the MD simulations of μ-KIIIA[C4A,C16A], removal of the Cys4−Cys16 disulfide restraint resulted in a change in conformation, consistent with its inability to bind VGSCs. Thus, the simulations have provided possible explanations for the varying importance of individual disulfide bonds in relation to the activity of μ-KIIIA on VGSCs. The structures from the MD simulations show exceptional similarity with the ensemble of experimentally derived NMR structures for both μ-KIIIA and μ-KIIA[C1A,C9A]. The high level of conformity between the experimental and theoretical structures confirms the utility of MD in the structural analysis of these small peptides.

Accumulating structural and functional studies, including this work, on the three μ-conotoxins, μ-SmIIIA, μ-SIIIA, and μ-KIIIA, provide us with an emerging picture of structural requirements of these peptides as blockers of VGSCs. An important conclusion is that the number of residues in the first loop has no significant effect on the overall conformations of the second and third loops that present critical residues. The second is that the μ-conotoxin scaffold can accommodate backbone spacers and/or removal of individual disulfide bridges without compromising bioactivity, emphasizing the adaptability of the μ-conotoxin scaffold and making it a valuable template for peptide engineering. Our results therefore have important implications for the future design of minimized analogues with greater subtype selectivity for use in the treatment of pain (*11*). It seems that the N-terminal region could be truncated to produce a minimized analogue which retains the key residues on the α-helical scaffold (-XXKWXRDHXR-). The success of MD simulations in reproducing the structures of μ-KIIIA and μ-KIIIA[C1A,C9A], as documented in Figure 5, implies that this approach will be a valuable adjunct to the process of designing truncated and stabilized analogues.

ACKNOWLEDGMENT

We thank Professor Jean Rivier for providing the synthetic peptides and Professor Alan Goldin for providing clones for $rNa_V1.2-1.5$ and $mNa_V1.6$, Prof. Gail Mandel for the $rNa_V1.7$ clone, and Dr. Layla Azam for cRNA preparations from these clones.

SUPPORTING INFORMATION AVAILABLE

Two tables of chemical shifts (KIIIA and KIIIA[C1A,C9A]) and eight figures (two figures of NMR spectra of KIIIA and KIIIA[C1A,C9A], four figures summarizing and comparing NOEs, angular parameters, and chemical shift data, and two figures of results of MD simulations). This material is available free of charge via the Internet at http://pubs.acs.org.

REFERENCES

1. French, R. J., and Terlau, H. (2004) Sodium channel toxins: Receptor targeting and therapeutic potential. *Curr. Med. Chem. 11*, 3053–3064.
2. Cummins, T. R., Sheets, P. L., and Waxman, S. G. (2007) The roles of sodium channels in nociception: Implications for mechanisms of pain. *Pain 131*, 243–257.
3. Catterall, W. A., Cestele, S., Yarov-Yarovoy, V., Yu, F. H., Konoki, K., and Scheuer, T. (2007) Voltage-gated ion channels and gating modifier toxins. *Toxicon 49*, 124–141.
4. Bulaj, G., Zhang, M. M., Green, B. R., Fiedler, B., Layer, R. T., Wei, S., Nielsen, J. S., Low, S. J., Klein, B. D., Wagstaff, J. D., Chicoine, L., Harty, T. P., Terlau, H., Yoshikami, D., and Olivera, B. M. (2006) Synthetic μO-conotoxin MrVIB blocks TTX-resistant sodium channel NaV1.8 and has a long-lasting analgesic activity. *Biochemistry 45*, 7404–7414.
5. Leipold, E., DeBie, H., Zorn, S., Borges, A., Olivera, B. M., Terlau, H., and Heinemann, S. H. (2007) μO conotoxins inhibit NaV channels by interfering with their voltage sensors in domain-2. *Channels 1*, 253–262.
6. Schmalhofer, W., Calhoun, J., Burrows, R., Bailey, T., Kohler, M. G., Weinglass, A. B., Kaczorowski, G. J., Garcia, M. L., Koltzenburg, M., and Priest, B. T. (2008) ProTx-II, a selective inhibitor of NaV1.7 sodium channels, blocks action potential propagation in nociceptors. *Mol. Pharmacol. 74*, 1476–1484.
7. Sokolov, S., Kraus, R. L., Scheuer, T., and Catterall, W. A. (2008) Inhibition of sodium channel gating by trapping the domain II voltage sensor with protoxin II. *Mol. Pharmacol. 73*, 1020–1028.
8. Norton, R. S., and Olivera, B. M. (2006) Conotoxins down under. *Toxicon 48*, 780–798.
9. Han, T. S., Teichert, R. W., Olivera, B. M., and Bulaj, G. (2008) *Conus* venoms: A rich source of peptide-based therapeutics. *Curr. Pharm. Des. 14*, 2462–2479.
10. Bulaj, G., West, P. J., Garrett, J. E., Watkins, M., Zhang, M. M., Norton, R. S., Smith, B. J., Yoshikami, D., and Olivera, B. M. (2005) Novel conotoxins from *Conus striatus* and *Conus kinoshitai* selectively block TTX-resistant sodium channels. *Biochemistry 44*, 7259–7265.
11. Zhang, M. M., Green, B. R., Catlin, P., Fiedler, B., Azam, L., Chadwick, A., Terlau, H., McArthur, J. R., French, R. J., Gulyas, J., Rivier, J. E., Smith, B. J., Norton, R. S., Olivera, B. M., Yoshikami, D., and Bulaj, G. (2007) Structure/function characterization of μ-conotoxin KIIIA, an analgesic, nearly irreversible blocker of mammalian neuronal sodium channels. *J. Biol. Chem. 282*, 30699–30706.
12. Green, B. R., Catlin, P., Zhang, M. M., Fiedler, B., Bayudan, W., Morrison, A., Norton, R. S., Smith, B. J., Yoshikami, D., Olivera, B. M., and Bulaj, G. (2007) Conotoxins containing nonnatural backbone spacers: Cladistic-based design, chemical synthesis, and improved analgesic activity. *Chem. Biol. 14*, 399–407.
13. Carrega, L., Mosbah, A., Ferrat, G., Beeton, C., Andreotti, N., Mansuelle, P., Darbon, H., De Waard, M., and Sabatier, J. M. (2005) The impact of the fourth disulfide bridge in scorpion toxins of the α-KTx6 subfamily. *Proteins 61*, 1010–1023.

14. Barnham, K. J., Torres, A. M., Alewood, D., Alewood, P. F., Domagala, T., Nice, E. C., and Norton, R. S. (1998) Role of the 6−20 disulfide bridge in the structure and activity of epidermal growth factor. *Protein Sci. 7*, 1738–1749.
15. Flinn, J. P., Pallaghy, P. K., Lew, M. J., Murphy, R., Angus, J. A., and Norton, R. S. (1999) Role of disulfide bridges in the folding, structure and biological activity of ω-conotoxin GVIA. *Biochim. Biophys. Acta 1434*, 177–190.
16. Pennington, M. W., Lanigan, M. D., Kalman, K., Mahnir, V. M., Rauer, H., McVaugh, C. T., Behm, D., Donaldson, D., Chandy, K. G., Kem, W. R., and Norton, R. S. (1999) Role of disulfide bonds in the structure and potassium channel blocking activity of ShK toxin. *Biochemistry 38*, 14549–14558.
17. Han, T. S., Zhang, M. M., Walewska, A., Gruszczynski, P., Cheatham, T. E., III, Yoshikami, D., Olivera, B. M., and Bulaj, G. (2008) Structurally-minimized μ-conotoxin analogs as sodium channel blockers: Implications for designing conopeptide-based therapeutics. *ChemMedChem,* in press.
18. Palmer, A. G., Cavanagh, J., Wright, P. E., and Rance, M. (1991) Sensitivity improvement in proton-detected 2-dimensional heteronuclear correlation NMR-spectroscopy. *J. Magn. Reson. 93*, 151–170.
19. Kay, L. E., Keifer, P., and Saarinen, T. (1992) Pure absorption gradient enhanced heteronuclear single quantum correlation spectroscopy with improved sensitivity. *J. Am. Chem. Soc. 114*, 10663–10665.
20. Gibbs, S. J., and Johnson, C. S. (1991) A PFG-NMR experiment for accurate diffusion and flow studies in the presence of eddy currents. *J. Magn. Reson. 93*, 395–402.
21. Dingley, A. J., Mackay, J. P., Chapman, B. E., Morris, M. B., Kuchel, P. W., Hambly, B. D., and King, G. F. (1995) Measuring protein self-association using pulsed-field-gradient NMR spectroscopy: Application to myosin light chain 2. *J. Biomol. NMR 6*, 321–328.
22. Yao, S., Howlett, G. J., and Norton, R. S. (2000) Peptide self-association in aqueous trifluoroethanol monitored by pulsed field gradient NMR diffusion measurements. *J. Biomol. NMR 16*, 109–119.
23. Piotto, M., Saudek, V., and Sklenar, V. (1992) Gradient-tailored excitation for single-quantum NMR spectroscopy of aqueous solutions. *J. Biomol. NMR 2*, 661–665.
24. Bartels, C., Xia, T. H., Billeter, M., Güntert, P., and Wüthrich, K. (1995) The program XEASY for computer-supported NMR spectral-analysis of biological macromolecules. *J. Biomol. NMR 6*, 1–10.
25. Seavey, B. R., Farr, E. A., Westler, W. M., and Markley, J. L. (1991) A relational database for sequence-specific protein NMR data. *J. Biomol. NMR 1*, 217–236.
26. Herrmann, T., Güntert, P., and Wüthrich, K. (2002) Protein NMR structure determination with automated NOE-identification in the NOESY spectra using the new software ATNOS. *J. Biomol. NMR 24*, 171–189.
27. Schwieters, C. D., Kuszewski, J. J., Tjandra, N., and Clore, G. M. (2003) The Xplor-NIH NMR molecular structure determination package. *J. Magn. Reson. 160*, 65–73.
28. Laskowski, R. A., Rullmannn, J. A., MacArthur, M. W., Kaptein, R., and Thornton, J. M. (1996) AQUA and PROCHECK-NMR: Programs for checking the quality of protein structures solved by NMR. *J. Biomol. NMR 8*, 477–486.
29. Koradi, R., Billeter, M., and Wüthrich, K. (1996) MOLMOL: A program for display and analysis of macromolecular structures. *J. Mol. Graphics 14*, 51–55, 29−32. .
30. Fiser, A., and Sali, A. (2003) Modeller: Generation and refinement of homology-based protein structure models. *Methods Enzymol. 374*, 461–491.
31. Keizer, D. W., West, P. J., Lee, E. F., Yoshikami, D., Olivera, B. M., Bulaj, G., and Norton, R. S. (2003) Structural basis for tetrodotoxin-resistant sodium channel binding by μ-conotoxin SmIIIA. *J. Biol. Chem. 278*, 46805–46813.
32. Lindahl, E., Hess, B., and van der Spoel, D. (2001) GROMACS 3.0: A package for molecular simulation and trajectory analysis. *J. Mol. Model. 7*, 306–317.
33. Jorgensen, W. L., and Tirado-Rives, J. (1988) The OPLS potential functions for proteins. Energy minimizations for crystals of cyclic peptides and crambin. *J. Am. Chem. Soc. 110*, 1657–1666.
34. Hess, B., Bekker, H., and Berendsen, H. J. C. (1977) LINCS: A linear constraint solver for molecular simulations. *J. Comput. Chem. 18*, 1463–1472.
35. Berendsen, H. J. C., Postma, J. P. M., DiNola, A., and Haak, J. R. (1984) Molecular dynamics with coupling to an external bath. *J. Chem. Phys. 81*, 3684–3690.
36. Daura, X., Gademann, K., Juan, B., Seebach, D., van Gunsteren, W. F., and Mark, A. E. (1999) Peptide folding: When simulation meets experiment. *Angew. Chem., Int. Ed. 38*, 236–240.
37. West, P. J., Bulaj, G., Garrett, J. E., Olivera, B. M., and Yoshikami, D. (2002) μ-Conotoxin SmIIIA, a potent inhibitor of tetrodotoxin-resistant sodium channels in amphibian sympathetic and sensory neurons. *Biochemistry 41*, 15388–15393.
38. Ellison, M., Feng, Z. P., Park, A. J., Zhang, X., Olivera, B. M., McIntosh, J. M., and Norton, R. S. (2008) α-RgIA, a novel conotoxin that blocks the α9α10 nAChR: Structure and identification of key receptor-binding residues. *J. Mol. Biol. 377*, 1216–1227.
39. Merutka, G., Dyson, H. J., and Wright, P. E. (1995) 'Random coil' ^{1}H chemical shifts obtained as a function of temperature and trifluoroethanol concentration for the peptide series GGXGG. *J. Biomol. NMR 5*, 14–24.
40. Zhang, M.-M., McArthur, J. R., Azam, L., Bulaj, G., Olivera, B. M., French, R. J., and Yoshikami, D. (2008) Synergistic and antagonistic interactions between tetrodotoxin and μ-conotoxin in blocking voltage-gated sodium channels. *Channels* , in press.
41. Schroeder, C. I., Ekberg, J., Nielsen, K. J., Adams, D., Loughnan, M. L., Thomas, L., Adams, D. J., Alewood, P. F., and Lewis, R. J. (2008) Neuronally selective μ-conotoxins from *Conus striatus* utilize an α-helical motif to target mammalian sodium channels. *J. Biol. Chem. 283*, 21621–21628.
42. Yao, S., Zhang, M. M., Yoshikami, D., Azam, L., Olivera, B. M., Bulaj, G., and Norton, R. S. (2008) Structure, dynamics and selectivity of the sodium channel blocker μ-conotoxin SIIIA. *Biochemistry 47*, 10940–10949.
43. Bayrhuber, M., Vijayan, V., Ferber, M., Graf, R., Korukottu, J., Imperial, J., Garrett, J. E., Olivera, B. M., Terlau, H., Zweckstetter, M., and Becker, S. (2005) Conkunitzin-S1 is the first member of a new Kunitz-type neurotoxin family. Structural and functional characterization. *J. Biol. Chem. 280*, 23766–23770.
44. Wang, C. Z., Zhang, H., Jiang, H., Lu, W., Zhao, Z. Q., and Chi, C. W. (2006) A novel conotoxin from *Conus striatus*, μ-SIIIA, selectively blocking rat tetrodotoxin-resistant sodium channels. *Toxicon 47*, 122–132.
45. Zhang, M. M., Fiedler, B., Green, B. R., Catlin, P., Watkins, M., Garrett, J. E., Smith, B. J., Yoshikami, D., Olivera, B. M., and Bulaj, G. (2006) Structural and functional diversities among μ-conotoxins targeting TTX-resistant sodium channels. *Biochemistry 45*, 3723–3732.
46. Wishart, D. S., Bigam, C. G., Holm, A., Hodges, R. S., and Sykes, B. D. (1995) ^{1}H, ^{13}C and ^{15}N random coil NMR chemical shifts of the common amino acids. I. Investigations of nearest-neighbor effects. *J. Biomol. NMR 5*, 67–81.
47. DeLano, W. L. (2002) The PyMOL Molecular Graphics System, DeLano Scientific, San Carlos, CA.

BI801998A